Frequency-selective excitation of guided acoustic modes in a photonic crystal fiber

B. Stiller,[1,*] M. Delqué,[1] J.-C. Beugnot,[1] M. W. Lee,[1] G. Mélin,[2]
H. Maillotte,[1] V. Laude,[1] and T. Sylvestre[1]

[1]*Institut FEMTO-ST, Université de Franche-Comté, CNRS UMR 6174, Besançon, France*
[2]*Draka, Route de Nozay, F-91460 Marcoussis, France*
birgit.stiller@femto-st.fr

Abstract: We present experimental and numerical results demonstrating the simultaneous frequency-selective excitation of several guided acoustic Brillouin modes in a photonic crystal fiber with a multi-scale structure design. These guided acoustic modes are identified by using a full vector finite-element model to result from elastic radial vibrations confined by the wavelength-scale air-silica microstructure. We further show the strong impact of structural irregularities of the fiber on the frequency and modal shape of these acoustic resonances.

References and links

1. R. M. Shelby, M. D. Levenson, and P. W. Bayer, "Guided acoustic-wave Brillouin scattering," Phys. Rev. B **31**, 5244–5252 (1985).
2. D. Elser, U. L. Andersen, A. Korn, O. Glöckl, S. Lorenz, C. Marquardt, and G. Leuchs, "Reduction of guided acoustic wave Brillouin scattering in photonic crystal fibers," Phys. Rev. Lett. **97**, 133901 (2006).
3. V. Laude, A. Khelif, S. Benchabane, M. Wilm, T. Sylvestre, B. Kibler, A. Mussot, J. M. Dudley, and H. Maillotte, "Phononic band-gap guidance of acoustic modes in photonic crystal fibers," Phys. Rev. B **71**, 045107 (2005).
4. P. Dainese, P. St. J. Russell, N. Joly, J. C. Knight, G. S. Wiederhecker, H. L. Fragnito, V. Laude, and A. Khelif, "Stimulated Brillouin scattering from multi-GHz-guided acoustic phonons in nanostructured photonic crystal fibres," Nat. Phys. **2**, 388–392 (2006).
5. N. Shibata, A. Nakazono, N. Taguchi, and S. Tanaka, "Forward Brillouin scattering in holey fibers," IEEE Photon. Technol. Lett. **18**, 412–414 (2006).
6. P. Dainese, P. St. J. Russell, G. S. Wiederhecker, N. Joly, H. L. Fragnito, V. Laude, and A. Khelif, "Raman-like light scattering from acoustic phonons in photonic crystal fiber," Opt. Express **14**, 4141–4150 (2006).
7. J.-C. Beugnot, T. Sylvestre, H. Maillotte, G. Mélin, and V. Laude, "Guided acoustic wave Brillouin scattering in photonic crystal fibers," Opt. Lett. **32**, 17–19 (2007).
8. G. S. Wiederhecker, A. Brenn, H. L. Fragnito, and P. St. J. Russell, "Coherent control of ultrahigh-frequency acoustic resonances in photonic crystal fibers," Phys. Rev. Lett. **100**, 203903 (2008).
9. M. S. Kang, A. Brenn, G. S. Wiederhecker, and P. St. J. Russell, "Optical excitation and characterization of gigahertz acoustic resonances in optical fiber tapers," Appl. Phys. Lett. **93**, 131110 (2008).
10. N. Nishizawa, S. Kume, M. Mori, T. Goto, and A. Miyauchi, "Symmetric and asymmetric fiber loop mirrors for observing guided-acoustic-wave Brillouin scattering in polarization-maintaining fibers," Opt. Lett. **19**, 1424–1926 (1994).
11. G. Mélin, L. Provost, A. Fleureau, S. Lempereur, X. Rejeaunier, E. Bourova, and L. Gasca, "Innovative design for highly non-linear microstructured fibers," in European Conference of Optical Communication (ECOC, 2004), p. Tu4.3.2.
12. A. Boucon, D. Alasia, J. Beugnot, G. Mélin, S. Lempereur, A. Fleureau, H. Maillotte, J. M. Dudley, and T. Sylvestre, "Supercontinuum generation from 1.35 to 1.7 μm by nanosecond pumping near the second zero-dispersion wavelength of a microstructured fiber," IEEE Photon. Technol. Lett. **20**, 842–844 (2008).
13. D. Royer and E. Dieulesaint, *Elastic Waves in Solids* (Springer, 2000), Vols. I and II.
14. R. N. Thurston, "Elastic waves in rods and clad rods," J. Acoust. Soc. Am. **64**, 1–37 (1978).

1. Introduction

When a coherent optical wave propagates through an optical fiber, it suffers phase noise due to the interaction with transverse acoustic waves that modulate the refractive index of the fiber. This effect, which is called guided acoustic wave Brillouin scattering (GAWBS), has been known since 1985 and considered for many years as detrimental to fiber-based standard and quantum communication systems [1]. In recent years there has been a renewed interest in the effect of GAWBS in photonic crystal fibers (PCFs) due to their remarkable ability to either suppress or enhance acoustic resonances, with the aim of using PCF for quantum optics or developing new efficient acousto-optic devices [2–4]. Recent works have indeed shown that GAWBS in PCF is radically different from conventional fibers and cannot be considered as a noise source. Instead, it leads to efficient phase modulation in the GHz range through the generation of high-frequency transverse acoustic waves trapped by the air-hole microstructure [2, 5–7]. It has also been reported that these ultra high-frequency acoustic resonances can be coherently controlled in PCF using laser pulses [8] or be turned into highly nonlinear artificial Raman oscillators [9]. In this work, we investigate GAWBS in a PCF with a multi-scale structure design and report the frequency-selective excitation of multiple high-frequency guided acoustic modes up to 2 GHz. Based on a full vector finite-element model (FEM), we show that these guided acoustic modes result from elastic radial vibrations selected by the wavelength-scale air-silica microstructure. The elasto-optic coefficient is calculated and is found to be in good agreement with the experimental GAWBS spectrum. We further show the strong impact of structural irregularities of the fiber on these transverse acoustic modes by numerically studying a perfectly symmetric air-hole structure designed from the real cross section of the PCF. Our results suggest that PCFs can be advantageously used to enhance and control guided acousto-optic interactions at ultra-high frequency by fiber design in view of potential applications for fiber-optic sensors or efficient acousto-optic devices.

2. Experiments

Polarized GAWBS in an optical fiber originates from radial elastic modes and leads to phase modulation and the appearance of a set of new frequencies in the wave spectrum [1]. To detect such an effect, we set up the fiber loop mirror depicted in Fig. 1 [10]. A distributed-feedback (DFB) Erbium-doped fiber laser at 1550 nm is amplified by an Erbium-doped fiber amplifier (EDFA) and amplified spontaneous emission (ASE) is removed by use of a 5 nm bandpass filter because it prevents the measurement of GAWBS. The output is then split into two counterpropagating beams and launched in the fiber loop mirror via a 50/50 fiber coupler. This loop mirror acts as an interferometer such that the two counterpropagating waves interfere destructively at the 50/50 fiber coupler and power is reflected to the port A. However, the two counterpropagating waves suffer phase modulation due to GAWBS and this small signal goes to the port B. The polarization controller and the polarizer are used to suppress the carrier wave as much as possible at port B and to maximize the GAWBS signal the RF spectrum. Finally the
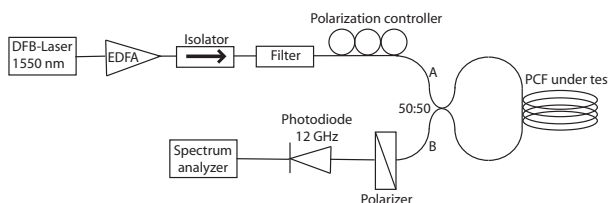

Fig. 1. Experimental setup for observing guided acoustic wave Brillouin scattering.

GAWBS spectrum is recorded by using a fast photodiode followed by a RF amplifier and an RF spectrum analyzer.

The PCF under test, illustrated in Fig. 2(c), consists of a multiscale microstructure with three different sizes of air holes and has a length of 106 m. The first two inner rows with 800 nm holes are based on a triangular lattice and define the fiber core and the single-mode propagation at 1550 nm, as confirmed by numerical simulations shown in Fig. 2(d). The two external rows consist of 12 larger elliptical holes and are intended to isolate the fiber core from the cladding to lower the intrinsic confinement losses [11]. This fiber actually exhibits two zero-dispersion wavelengths and a high nonlinear coefficient ($25\,W^{-1}km^{-1}$) and has been used for supercontinuum generation [12]. Figure 2(a) shows the GAWBS spectrum. Several sideband frequency peaks are observed from 200 MHz to 2 GHz and, in particular, three dominant acoustic modes at 410 MHz, 915 MHz and 1940 MHz. Above 2 GHz no other acoustic modes appear. This multi-frequency spectrum is different from the single-mode spectrum previously observed in standard triangular-lattice PCF [6, 7].
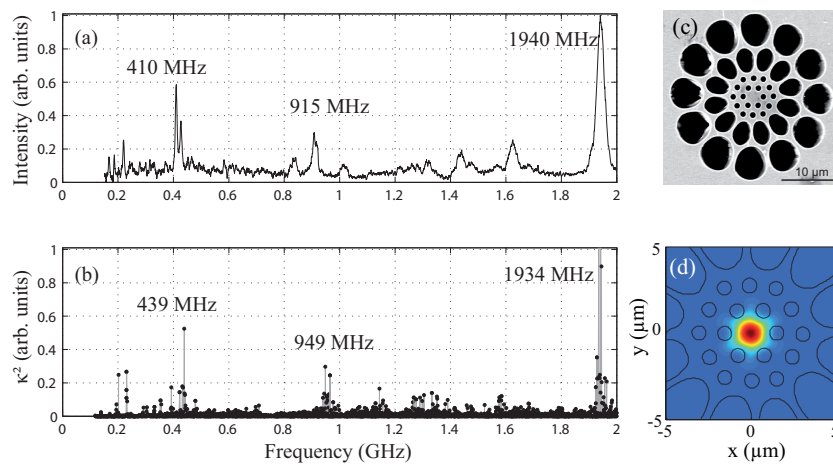

Fig. 2. (a) Experimental RF spectrum showing the guided acoustic modes of the photonic crystal fiber shown in (c). (b) FEM-based numerical simulation of the elasto-optic coefficient κ^2 as a function of the acoustic frequency. (c) scanning electron microscope (SEM) image of the PCF cross-section: core diameter 2.4 μm, diameter of small holes 820 nm, diameter of middle holes 3.6 μm, diameter of big holes 5.1 μm. (d) fundamental optical mode solved at 1550 nm using FEM simulation. Air-holes contour lines are depicted in black.

3. GAWBS model

To identify guided acoustic modes in the PCF, we have performed FEM-based numerical simulations of the optical and acoustic modes using the COMSOL Multiphysics software. For this purpose, the PCF cross-section has been imported from a scanning electron microscope (SEM) image and transformed to a finite element mesh. We have used the RF module to solve the optical mode and a custom partial differential equation model for full-vector 3D acoustic modeling. As acoustic constants, we used silica density $\rho = 2203\,kg.m^{-3}$, Young's modulus $E_Y = 73.1\ 10^9\,Pa$, and Poisson ratio $v_P = 0.17$. The optical refractive index of silica is $n = 1.444$. Single-mode optical propagation was found at 1550 nm, with an effective refractive index $n_{\text{eff}}(1550\ nm) = 1.392$. The fundamental optical mode is shown as a color plot in Fig. 2(d). Both the optical and acoustic modal shapes are then combined to estimate the elasto-optic

diffraction coefficient κ that is written as [3]:

$$\kappa = \int_\sigma dxdy E_i E_j p_{ijkl} S_{kl}. \tag{1}$$

In this expression, σ is the transverse section of the fiber, E_i and E_j are the pump and scattered optical modes, respectively, p_{ijkl} is the strain-optical tensor, and S_{kl} is the acoustic strain tensor. The Einstein summation convention on repeated indices is employed. κ^2 is proportional to the scattering efficiency and thus models the GAWBS spectrum. The result is depicted in Fig. 2(b). Three main peaks are found, in good agreement with Fig. 2(a), both with respect to modal frequencies and relative scattering efficiencies. The small discrepancy of acoustic frequencies can be attributed to scaling errors on the SEM image. In order to investigate more clearly the acoustic modes trapped by the air-hole microstructure, we compute the strain energy density (SED) as [13]

$$W_s = \frac{1}{2} \left(\frac{\partial u}{\partial x} T_{xx} + \frac{\partial v}{\partial y} T_{yy} + (\frac{\partial u}{\partial y} + \frac{\partial v}{\partial x}) T_{xy} \right), \tag{2}$$

where (u, v, w) and T_{kl} are the displacements and stresses of the FEM solution, respectively. We also calculate the kinetic energy density (KED) as [13]

$$E = \frac{1}{2} \rho \omega^2 \left(u^2 + v^2 + w^2 \right), \tag{3}$$

with ω the angular frequency of the acoustic mode and ρ the density. The SED and KED of the three main acoustic modes are plotted in Figs. 3(a-c) and (d-f), respectively. It is clearly seen that the three acoustic modes are spatially confined within the first external row of the fiber (the big core), the second internal row, and the fiber core (small core), respectively. As GAWBS is the signature of the scattering of the incident optical mode by acoustically-induced strain, the scattering efficiency κ is expected to be higher for a strong overlap between the SED and the optical mode. This is clearly apparent for the highest frequency mode at 1934 MHz in Fig. 3(c). Note that the small peaks around 200 MHz seen in both Figs. 2 (a) and (b) were also analyzed and were attributed to the modes confined to the second (outermost) external row. It is seen from Figs. 3(a-f) that both the SED and KED are not symmetrically distributed due to structural irregularities of the PCF.

To get further insight, we have performed numerical simulations for a model PCF without any structural irregularity. For this purpose, we have designed a fiber cross-section representing the same microstructure as in Fig. 2(c) but with defect-less holes, pitches and angles. The resulting scattering efficiency is plotted in Fig. 4(a) and is similar to that of Fig. 2(b). Of particular interest are the three main acoustic resonance peaks now appearing at unique frequencies, whereas those computed for the real structure degenerate in several peaks with close frequencies (see, e.g., the 950 MHz peak in Fig. 2(b) which is composed of five adjacent modes). The structural irregularities of the fiber actually remove the degeneracy of acoustic modes and the multimodal nature of the real structure originates from an energy splitting (or frequency splitting) of the acoustic modes. In this way, we can interpret the spectral width of GAWBS peaks as resulting not only from the acoustic lifetime (related to acoustic propagation losses) but also from transverse structural irregularities of the fiber cross-section.

The SED and KED of the three main acoustic modes of the model PCF are shown in Figs. 5(a-c) and (d-f), respectively. In contrast to Fig. 3, both energy density distributions are now symmetric. This clearly demonstrates the strong impact of structural irregularities of the PCF on guided acoustic modes and their frequencies. The SED in Figs. 5(a-c) confirms the efficient overlap between the strain field and the optical mode. The low-frequency mode in Fig. 5(a) can be understood as a circularly symmetric mode of the big core, whereas the middle- and
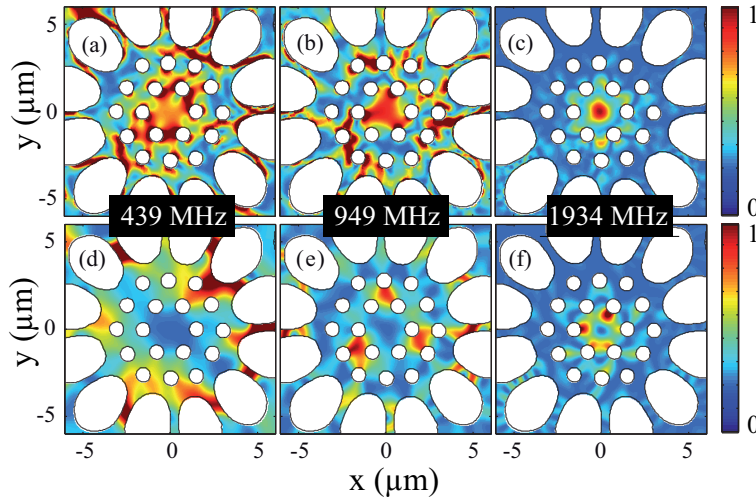
Fig. 3. Numerical calculation (color plot) of the strain energy density distribution (a-c) and the kinetic energy density (d-f) of the 439, 949 and 1934 MHz acoustic modes.

high-frequency modes in Figs. 5(b,c) can be identified as $2\pi/6$-symmetric modes limited to the second internal row and the optical core, respectively. The fact that the structure in the middle is triangular enhances these $2\pi/6$-symmetric modes contrary to the quasi-circular distribution of the first large holes surrounding the big core. In this way, the big core nearly behaves like a silica rod. This can be quantitatively verified by the relation $v = c_{R01} \cdot V_T/D$ which links the frequency v of the fundamental elastic mode to the rod diameter D by a constant $c_{R01} \cdot V_T$, where $V_T = 3740$ m/s is the transverse acoustic velocity and c_{R01} is a factor which depends on the acoustic mode, in this case the fundamental R_{01}-mode.
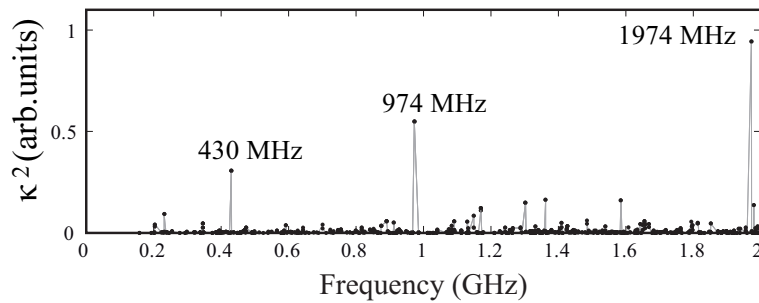

Fig. 4. Elasto-optic coefficient as a function of the acoustic frequency for the perfect microstructure.

The product $c_{R01} \cdot V_T$ is equal to $3.82 \cdot 10^3$ m/s (equivalent to the factor q in [9]) and was obtained from simulation but also by solving the Pochhammer-Chree relations [14] that depend on both the transverse acoustic velocity V_T and the longitudinal acoustic velocity $V_L = 5996$ m/s. The latter analytic solution leads to $v = c_{R01} \cdot V_T/D \approx 3.205/\pi \cdot V_T/D = 3.82 \cdot 10^3/D$, in good agreement with the numerical simulation. Consequently, the constant $c_{R01} \cdot V_T$ can be seen as an effective acoustic velocity that depends on both the transverse and longitudinal acoustic velocities. For the radial mode with the lowest frequency, at 410 MHz, the rod diameter can be estimated from the above expression to 8.7 μm, in excellent agreement with the diameter
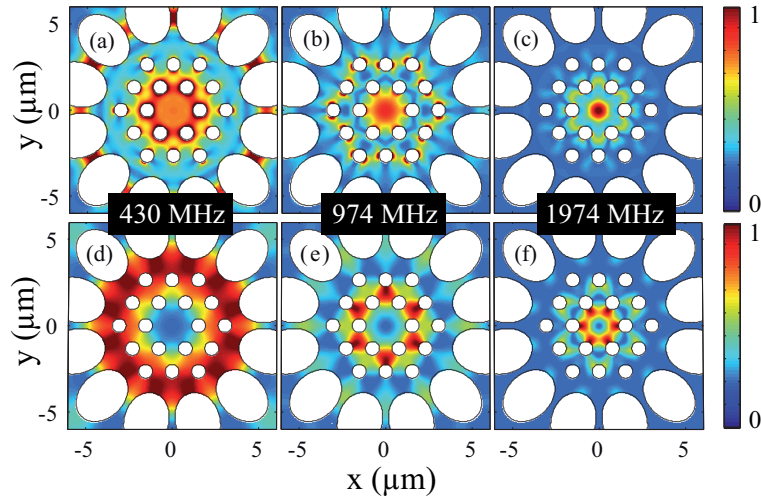
Fig. 5. Numerical simulations (color plot) of a perfect PCF design without any structural irregularity. (a-c) strain energy density distribution and (d-f) elastic energy distribution of the 430, 974 and 1974 MHz acoustic modes confined to the microstructure, respectively.

measured on the SEM image. This suggests that the GAWBS spectrum can be used to provide an accurate measurement of the dimensions of the PCF core. However, this conclusion is not valid for the middle- and the high-frequency modes at 915 MHz and 1940 MHz, because these exhibit $2\pi/6$-symmetry and thus cannot be identified as fundamental rod modes.

4. Conclusion

Guided acoustic wave Brillouin scattering has been investigated in a photonic crystal fiber with a multiscale structure. It has been shown both experimentally and numerically that such air-silica microstructure supports the simultaneous frequency-selective excitation of several transverse guided acoustic modes with frequencies up to 2 GHz. We provided a complete numerical analysis of these acoustic resonances whose frequencies are found to be strongly related to the air-hole microstructure of the fiber. We further demonstrated the impact of structural irregularities of the fiber on guided acoustic modes. Our results suggest that photonic crystal fibers can be advantageously used to enhance and control guided acousto-optic interactions at ultra-high frequency in view of potential applications for fiber-optic sensors or acousto-optic devices.